PCCP

Dynamic Article Links

Cite this: *Phys. Chem. Chem. Phys.*, 2011, **13**, 17712–17721

www.rsc.org/pccp

PAPER

A modular molecular photovoltaic system based on phospholipid/alkanethiol hybrid bilayers: photocurrent generation and modulation†

Hong Xie, Kai Jiang and Wei Zhan*

Received 25th May 2011, Accepted 22nd August 2011
DOI: 10.1039/c1cp21701a

Monolayer quantities of 1-palmitoyl-2-oleoyl-*sn*-glycero-3-phosphocholine (POPC), incorporated with either fullerenes or ruthenium tris(bipyridyl) ($Ru(bpy)_3^{2+}$) complexes, were formed on ferrocene-terminated C11-alkanethiol self-assembled monolayers (SAMs) through lipid fusion. Thus formed hybrid structures are characterized by quartz crystal microbalance, UV-vis spectroscopy, cyclic voltammetry and impedance analysis. In comparison to lipid monolayers deposited on C12-alkanethiol SAMs, photocurrent generation from these ferrocene-based structures is significantly modulated, displaying attenuated anodic photocurrents and enhanced cathodic photocurrents. While a similar trend was observed for the two photoagents studied, the degree of such modulations was always found to be greater in fullerene-incorporated bilayers. These findings are evaluated in the context of the film structure, energetics of the involved photo(electrochemical) species and cross-membrane electron-transfer processes.

1. Introduction

A multicomponent photocurrent generation system, based on photoactive agents (either fullerene or ruthenium tris(bipyridyl) (bipyridyl = 2,2′-bipyridine) species) and ferrocene co-assembled in a hybrid lipid bilayer, is described here. In both cases, it is found that the presence of a ferrocene layer in between the photoactive layer and the electrode can significantly modulate the observed photocurrents, leading to an enhanced cathodic current and an attenuated anodic current. This work presents an alternative strategy of organizing multiple photo-/redox-active agents on electrodes for photocurrent generation and may also provide a modular model system for studying photoinduced electron transfer across lipid membranes.

There has been a lasting research interest[1–3] in mimicking natural photosynthesis using synthetic approaches and for over three decades, lipid-bilayer based structures[4,5] have been employed in building such biomimetic systems. Because lipid bilayers typically are only 3–5 nm thick, electron tunneling and photoinduced electron transfer across the lipid membrane can occur under favorable conditions. Calvin and his coworkers[6] were among the first to recognize the utility of lipid bilayers in building artificial photosynthetic systems. By using liposomes, for example, they showed that efficient photosensitized electron transfer across a lipid bilayer could be established between membrane-bound ruthenium tris(bipyridyl) complexes and aqueous viologen and EDTA.[7,8] Using surfactant vesicles and black lipid membranes (BLMs), Fendler and coworkers[9,10] produced a series of biomimetic photosynthetic systems in the 1980–90s. Specifically, photovoltages could be reliably generated across BLMs[11] decorated with photoactive CdS particles. In still another approach, Gust, Moore and Moore[12,13] demonstrated that a quinone–porphyrin–carotene triad conjugate could be reconstituted in liposomes and upon light excitation, this synthetic complex could drive the production of proton potential[14] as well as ATP synthesis[15] at the liposome hosts. These results, together with numerous others,[4,5,16] clearly point to the usefulness and versatility of liposomes and BLMs in building artificial photosynthetic systems.

Continuing research in membrane biophysics and biotechnology has brought forth new lipid-bilayer structures in recent years. For example, the work of McConnell,[17,18] Boxer,[19,20] Sackmann[21,22] and others has established that well-defined lipid bilayers can be formed on hydrophilic substrates such as glass and oxidized silicon. Structurally, these bilayers are symmetrical, with controllable fluidity, and stable over a long period of time (*i.e.*, hours or longer) when immersed in aqueous media, which warrants their use as a model of cellular membranes. More recently, it has also been shown that a monolayer of lipids can be deposited on a pre-formed self-assembled monolayer, thus producing a hybrid bilayer structure[23–25] on a solid support. Several types of hybrid bilayers have been successfully constructed on alkane/lipid SAMs on gold[26,27] as well as oxide substrates.[28,29] Importantly, since these bilayers are formed in two separate steps, it becomes possible to control the chemical makeup of each leaflet of the bilayer.

Department of Chemistry and Biochemistry, Auburn University, Auburn, AL 36849, USA. E-mail: wzz0001@auburn.edu; Tel: +1 (334) 844-6984

† Electronic supplementary information (ESI) available. See DOI: 10.1039/c1cp21701a

We have been interested in building new artificial photosynthetic systems with these solid-supported lipid-bilayer structures.[30–32] With improved stability and controllable bilayer architecture, these structures potentially provide new opportunities for us to study photoinduced electron transfer processes in a well-defined lipid environment. In particular, because these structures allow various photoactive species to be directly organized/immobilized on electrodes, the efficiencies of electron transfer and photoconversion can be directly monitored through detection of photocurrents. Exploring this new approach, we have recently built single- as well as multicomponent photoconversion systems,[30–32] based on several photoactive species immobilized on electrode-supported lipid bilayers.

Continuing this lipid-based approach, we report herein that a ferrocene monolayer inserted in between a photoactive lipid monolayer and an underlying electrode can significantly modulate the photocurrents. Photocurrents generated from both $Ru(bpy)_3^{2+}$ and fullerene are studied and compared on otherwise identical bilayer structures. These results are evaluated in terms of the energetics and relative position of the photo-/redox-active species within the bilayers.

2. Experimental section

2.1 Reagents

Phospholipids such as 1-palmitoyl-2-oleoyl-*sn*-glycero-3-phosphocholine (POPC) and 1,2-dioleoyl-*sn*-glycero-3-phosphoethanolamine (DOPE) were obtained from Avanti Polar Lipids. Synthesis of monomalonic fullerene (C_{63})[30] and $Ru(bpy)_3^{2+}$-conjugated[31] DOPE was reported previously. 11-Ferrocenyl undecanethiol (FcC11SH) was received from Dojindo Co. and used without further purification. Sodium sulfate and sodium perchlorate were obtained from Fisher Scientific. Other reagents, including dodecanethiol (C12SH), chlorophyll *a* (from spinach), 4-(2-hydroxyethyl)piperazine-1-ethanesulfonic acid (HEPES), methyl viologen dichloride hydrate (MV^{2+}), hexaamine ruthenium (III) chloride, tetrabutylammonium tetrafluoroborate (Bu_4NBF_4, 99%), L(+)-ascorbic acid sodium salt (sodium ascorbate), D-(+)-glucose, glucose oxidase (type X-S, from *Aspergillus niger*) and catalase (from bovine liver), were obtained from Sigma-Aldrich. Tetrahydrofuran (THF, Reagent ACS grade) is from J. T. Baker, Inc. All aqueous solutions employed in these experiments were prepared using 18.2 MΩ cm deionized water (Millipore).

2.2 Monolayer and hybrid bilayer preparation

Gold-coated substrates were fabricated by sputtering gold (thickness: 100 nm) onto chromium-coated (thickness: 100 nm) silicon wafers. Prior to the self-assembly of alkanethiol monolayers, the gold-coated substrates were cleaned in piranha solution (3 : 1 v/v concentrated H_2SO_4/30% H_2O_2 solution) for 15 min and then thoroughly rinsed with water and ethanol and dried in an argon stream. The cleaned gold electrodes were incubated in the ethanol solutions of 1 mM thiols (C12SH, Fc-C11SH or their 1 : 1 mol mixture) at room temperature typically for >15 h. After that, the SAM-modified gold substrates were carefully rinsed with ethanol and DI water, dried in argon, and then assembled in the Teflon cell for further use.

Liposomes of various compositions are prepared by an extrusion method as previously described.[30] Briefly, appropriate quantities of lipids in chloroform were thoroughly mixed and dried to a film by rotary evaporation. This mixture was then sonicated (Bransonic, model: 3510-DTH) in HEPES buffer (10 mM HEPES, 100 mM Na_2SO_4, pH 7.7) at room temperature for 2 h. The resulting solution was then extruded consecutively through polycarbonate membranes (Nuclepore, Whatman) of 400 and 80 nm-diameter pores at room temperature. The total lipid concentration of the final product was approximately 2 mM. The exact compositions of lipids used in the preparation are specified in the main text.

To form the SAM/lipid hybrid bilayers, typically a 300 μL of liposome solution with a total lipid concentration of 1 mM was added onto the SAM fixed in a Teflon cell and incubated at room temperature for 2 h. The unbound liposome solution was then removed from the cell by exchanging with HEPES buffer solution (10 mM HEPES, 100 mM Na_2SO_4, pH 7.7) at least 20 times.

2.3 Quartz crystal microbalance (QCM)

QCM measurements were performed on a QCM analyzer equipped with a 5 MHz crystal oscillator (Model QCM25, Stanford Research Systems) at room temperature. The gold-coated quartz crystals were cleaned in piranha solution for 3 min and then rinsed with a copious amount of water and ethanol and dried in argon. Thus cleaned crystals were incubated in the ethanol solutions of 1 mM thiols (C12SH or Fc-C11SH) at room temperature for at least 15 h and then rinsed with ethanol and DI water, and dried in argon. These SAM-covered gold crystals were then mounted onto the QCM oscillator connected to a flow cell. HEPES buffer (10 mM HEPES, 100 mM Na_2SO_4, pH 7.7) was first flowed through the cell until a steady frequency baseline was obtained (*i.e.*, $\Delta f < 1.0$ Hz over 10 min). To initiate the lipid deposition on the SAMs, POPC liposome solutions of approximately 0.15 mM total lipids were flowed into the cell. Switching of solutions delivered to the gold-coated QCM crystals was realized by the flow cell controlled by a peristaltic pump.

2.4 UV-vis absorption spectroscopy

UV-vis spectra were acquired with a UV-visible spectrophotometer (Cary 50 Bio, Varian). To obtain absorption spectra of chlorophyll *a* in hybrid bilayers, a home-machined Teflon cell was fitted to the sample holder of the same spectrometer and so optically aligned. The cell is configured to have an all-through liquid reservoir that can be sandwiched between two planar substrates, one of which is a semi-transparent gold substrate (10 nm Au coated on glass slides, Sigma-Aldrich) and the other microscope cover slides (VWR).

2.5 Impedance analysis

The impedance of the alkanethiol monolayer and the lipid/alkanethiol hybrid bilayer was measured with an SI 1260 impedance/gain-phase analyzer (Solartron). The measurements were carried out on a two-electrode setup, which comprises a gold film electrode covered with a monolayer (or a bilayer) and a Ag/AgCl (saturated KCl) electrode in

10 mM $NaClO_4$ aqueous solution. Throughout the measurements, the gold electrodes were poised at 0.0 V *vs.* Ag/AgCl, on which a sinusoidal ac wave of 10 mV is superimposed. The obtained data were fitted to an equivalent circuit consisting of a resistor (the electrolyte solution) and a capacitor (the surface bound layers) connected in series using the included analysis software package (ZView).

2.6 Fluorescence spectroscopy

The fluorescence emission spectra of $Ru(bpy)_3^{2+}$-containing hybrid bilayers on 10 nm gold-coated glass slides (Sigma-Aldrich) were acquired using a PI Acton spectrometer (SpectraPro SP 2356, Acton, NJ) that is connected to the side port of an epifluorescence microscope (Nikon TE-2000U, Japan). The emission signal was recorded by a back-illuminated digital CCD camera (PI Acton PIXIS:400B, Acton, NJ) operated by a PC. The excitation was generated by a mercury lamp (X-Cite 120, EXFO, Ontario, Canada) filtered by a band-pass filter at 470 ± 20 nm. The emission signal was filtered by a long-pass filter with a cutoff wavelength of 515 nm.

2.7 Electrochemistry and photoelectrochemistry

The electrochemical and photoelectrochemical measurements were carried out in a three-electrode Teflon photoelectrochemical cell containing SAM-covered gold substrates (with/without a lipid bilayer) as the working electrode, a Pt wire as the counter electrode and Ag/AgCl (in saturated KCl) as the reference electrode. Cyclic voltammetry experiments were carried out in 1 mM hexaamine ruthenium(III) chloride in 100 mM $NaClO_4$ with a potentiostat (CHI 910B, CH Instruments). The scan rate was 100 mV s^{-1}.

Different solutions were employed in the anodic and cathodic photocurrent generation. For the anodic process, 50 mM ascorbate in a buffer (10 mM HEPES, 100 mM Na_2SO_4, pH 7.7) was used; whereas 50 mM methyl viologen in 100 mM Na_2SO_4 electrolyte solution was used in the cathodic process. The cell was irradiated with light from a Hg lamp (X-Cite, series 120 PC, EXFO) filtered at 470 ± 20 nm for $Ru(bpy)_3^{2+}$-based devices (average intensity: 20 mW cm^{-2}) and at 417 ± 30 nm for fullerene-based systems (average intensity: 40 mW cm^{-2}). In the case of anodic current generation, oxygen in the cell was removed by adding 50 mM glucose, 50 units mL^{-1} glucose oxidase, and 200 units mL^{-1} catalase in the solutions. To obtain the photocurrent action spectra, the bilayer samples were irradiated with monochromatic light from a Xe lamp (100 W) and the resulting photocurrents were recorded on a potentiostat (CHI 910B, CH Instruments). The variation of excitation light intensity at different wavelengths was corrected with a photometer (Thorlabs).

3. Results and discussion

3.1 Formation of SAM/lipid hybrid bilayers

The formation of SAM/lipid hybrid bilayers on gold substrates is carried out in two steps (Scheme 1). First, a SAM of either dodecanethiol (C12SH) or 11-ferrocenyl-1-undecanethiol (Fc-C11SH) is formed on clean gold substrates. In the second step, a monolayer of phospholipids (*e.g.*, 1-palmitoyl-2-oleoyl-*sn*-glycero-3-phosphocholine, POPC) is deposited on the pre-formed SAM *via* lipid fusion,[23,31] which is achieved by exposing the SAM to a POPC liposome solution for a certain period of time (see the Experimental section). This step also serves to decorate the bilayer with the photoactive agents, $Ru(bpy)_3^{2+}$ or fullerene, which are separately incorporated into the POPC matrix in the liposome preparation step.[30,31] Structurally, this sequential formation of the bilayer enables a directional organization of photo-/redox-active agents and ferrocene on the electrode, since the ferrocene moieties are fixed on the SAM and the photoagents are primarily associated with the top lipid layer.

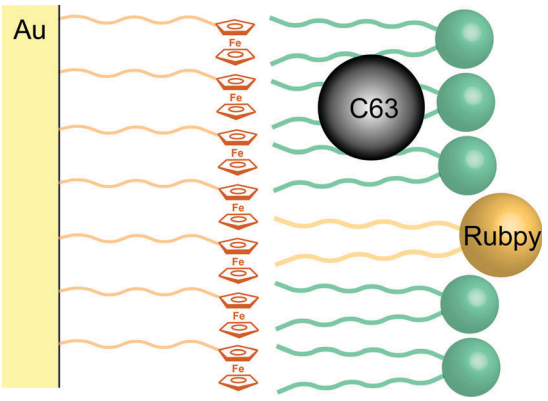

Scheme 1 Graphical layout of the multicomponent photocurrent-generating system constructed on hybrid bilayers. The hybrid bilayers comprise a ferrocenyl-terminated SAM and an upper lipid monolayer assembled with either fullerene or $Ru(bpy)_3^{2+}$. This cartoon does not imply the actual organization or stoichiometry of involved species in the bilayers.

3.2 Characterization of ferrocene–SAM/lipid hybrid bilayers

Four techniques were employed to characterize the deposition of lipids on pre-formed C12SH and Fc-C11SH SAMs: quartz crystal microbalance (QCM), UV-vis absorption spectroscopy, cyclic voltammetry, and impedance analysis. Fig. 1 shows the result of the QCM measurement, where the C12SH and Fc-C11SH SAMs were formed on gold-coated quartz crystals and the oscillation frequency shifts of these crystals were then used to monitor the deposition of lipids on corresponding SAMs. While a similar deposition profile was observed for the two SAMs when exposed to a POPC liposome solution, the frequency decrease associated with lipid deposition on the C12SH SAM was always found to be slightly larger: ~320 Hz *vs.* ~300 Hz for the Fc-C11SH SAM. According to the Sauerbrey equation,[33,34] $\Delta f = -C_f \Delta m$, this result indicates that a slightly larger amount of POPC is deposited on the C12SH SAM than on the Fc-C11SH SAM. For both SAMs, however, the magnitude of the frequency shifts would also suggest the formation of lipid multilayers, rather than a monolayer. Deviations from the ideal Sauerbrey behavior have been observed experimentally, which can be attributed to several factors,[33,35,36] such as the viscoelastic effect, surface roughness, interfacial liquid properties, and the stiffness of the film on the electrode. In a revealing study,[37] Ha and Kim evaluated the relative significance of these factors using a modified four-layer QCM model. In their case,

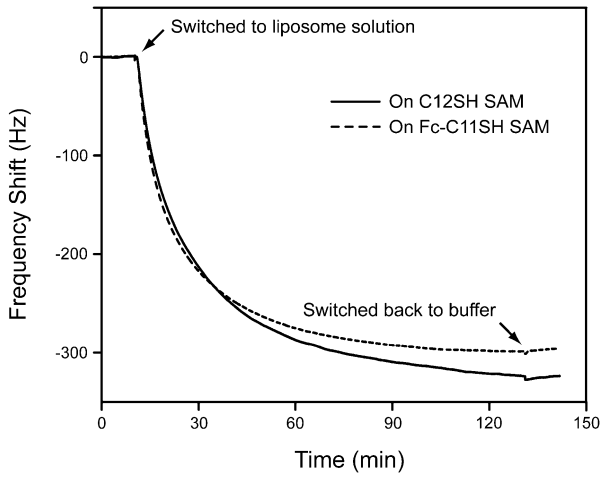

Fig. 1 QCM monitoring of lipid deposition on either the C12SH SAM (solid trace) or the Fc-C11SH SAM (dashed trace). Arrows indicate the times at which the solutions were switched from buffer (10 mM HEPES, 100 mM Na_2SO_4, pH 7.7) to a POPC liposome solution (0.15 mM POPC in the same buffer) and then back.

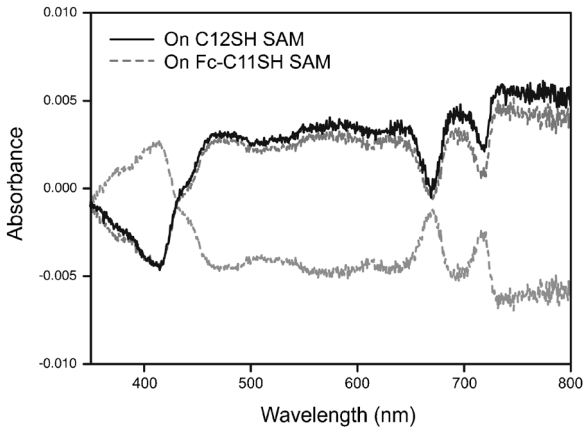

Fig. 2 UV-vis spectra of 5% (mol) chlorophyll *a* in the POPC layer formed on either the C12SH SAM (solid trace in black) or the Fc-C11SH SAM (dashed trace in gray). For clarity, the spectrum in gray was also inverted and offset in the figure. To form such bilayers, POPC liposomes ($\sim$1 mM in HEPES buffer saline) incorporated with 5% chlorophyll *a* were incubated with the SAMs for 2 h. See the Experimental section for more details.

frequency shifts as large as 1000–2000 Hz were recorded when lipid vesicles were deposited on a C18SH SAM, whereas the accompanying ellipsometry measurement indicated exclusively monolayer formation. This large decrease in frequency was primarily attributed to a substantial increase in the viscosity of the liquid layer adjacent to the QCM electrode. When a monolayer of lipids was formed on top of the SAM, it alters the hydrophobicity of the surface and thus modifies the organization of the water layer near the electrode. To a less extent, the change of interfacial slippage conditions during lipid deposition can also cause the oscillation frequency to decrease.

On the other hand, the formation of alkanethiol-SAM/phospholipid hybrid bilayers, under conditions similar to ours, has been well established and characterized.[23–25] Since the deposition profiles obtained on the C12SH SAM and the Fc-C11SH SAM are rather similar, it is tentatively concluded that a monolayer, or close-to-monolayer, amount of POPC can be deposited on the Fc-C11SH SAM. As shown below, this conclusion is generally supported by other characterization results.

3.3 UV-vis absorption spectroscopy

Taking advantage of the exceedingly high absorptivity of chlorophyll *a* (ε_{430}, ε_{660}: 1.1×10^5, 8.6×10^4 M^{-1} cm^{-1} in diethyl ether, for example)[38] and its high dispersity in lipid-based matrices,[39] we formed bilayers containing chlorophyll *a* at the top lipid layer, whose absorption response was then used to quantify the amount of deposited lipids on C12SH and Fc-C11SH SAMs. In order for this quantification method to be valid, it is necessary to assume that the deposition of chlorophyll *a* on SAMs proceeds quantitatively, that is, proportional to its loading level in liposomes. As shown in Fig. 2, for lipid layers deposited on both SAMs, the absorbance of associated chlorophyll *a* appears closely comparable. This result thus suggests that a lipid monolayer can be formed on a pure ferrocenyl-terminated SAM similar to alkanethiol SAMs. This observation is consistent with the formation mechanism[40,41] of SAM/lipid hybrid bilayers, which is largely driven by the hydrophobic/hydrophobic interaction between the hydrocarbon portions of the two materials. The fact that a lipid monolayer can be formed on the two SAMs almost non-discriminatorily indicates that such a bilayer formation may take place as long as the terminal group of the underlying SAM is hydrophobic.

3.4 Electrochemistry

Cyclic voltammetry (CV) was used to monitor the formation of C12SH and Fc-C11SH SAMs on gold substrates. As shown in Fig. 3, a quasi-reversible voltammogram was obtained on a bare gold surface using ruthenium hexaamine as a probe.

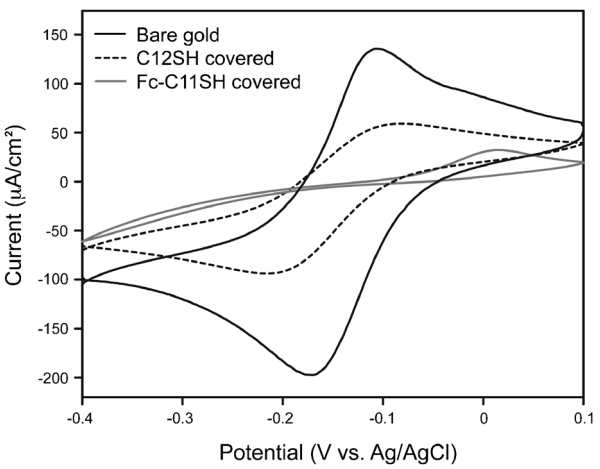

Fig. 3 Voltammetric characterization of formation of C12SH and Fc-C11SH SAMs on gold electrodes. A deaerated solution containing 1 mM $Ru(NH_3)_6^{3+}$ in 0.1 M $NaClO_4$ was probed with gold film electrodes covered with different SAMs. A three-electrode setup with a Ag/AgCl reference electrode and a Pt counter electrode was used; scan rate: 100 mV s^{-1}.

Formation of SAM films on gold blocks the access of probe molecules to the electrode surface, thus resulting in decreased voltammetric responses. Noticeably, a higher level of blocking was observed on the Fc-C11SH SAM as compared to the C12SH SAM, which may be caused by the relatively bulky ferrocene moiety in Fc-C11SH that can separate the solution redox molecules farther away from the gold electrode as compared to C12SH. Compared to another probe, ferricyanide, we used previously, the level of blocking by the C12SH SAM is noticeably less when ruthenium hexaamine is used. This result indicates that the latter is a more sensitive probe for checking integrity of SAMs and also points to the fact that the SAMs studied here are not defect-free.

Cyclic voltammetry was also performed on the Fc-C11SH SAMs before and after lipid adsorption (Fig. 4), as well as in THF (Fig. S1, ESI†). For the pure ferrocene-covered SAM, a broad, nearly symmetrical oxidation/reduction wave was apparent, *i.e.*, $E_{pa}(E_{pc}) = 0.39(0.38)$ V *vs.* Ag/AgCl. Integration of the charges associated with the voltammogram gives a ferrocene coverage of 2.2×10^{14} molecules cm^{-2}, consistent with a monolayer formation on gold.[42,43] Decorating this SAM with a layer of POPC produces a drastic change in the resulting CV. In particular, the onset of the oxidation wave is shifted positively by more than 100 mV and once the onset is reached, additional increase of the applied potential gives rise to a sharp oxidation wave. Despite this significant difference, the integrated charges from the two CVs appear reasonably close, *i.e.*, 1.8×10^{14} molecules cm^{-2} for the lipid-covered SAM. The cathodic wave is similarly modified. While the E_{pa} almost stays unchanged, there is a ~ -40 mV shift in E_{pc}. Additional measurements were also conducted on the 1 : 1 C12SH/Fc-C11SH mixed SAM with/without the POPC top layer. Similar to the pure ferrocene SAM, the CV of the mixed SAM is broad and nearly symmetrical. Once it is covered with POPC, however, the CV response becomes narrowed and the oxidation peak is further shifted to a more positive potential, *i.e.*, 0.48 V. In THF, the CV of the pure Fc-C11SH SAM features a positively shifted onset of the oxidation potential (as compared to that of the POPC-covered Fc-C11SH SAM in water) and a large ΔE_p of nearly 200 mV (ESI†, Fig. S1), which indicates significant reorganization of ferrocene moieties in this solvent during reduction/oxidation. For the 1 : 1 C12SH/Fc-C11SH mixed SAM, the positive potential shift (as compared to that of the Fc-C11SH SAM) is still observed but appears less pronounced than in the case of lipid-covered SAMs probed in water, especially in the oxidation scan.

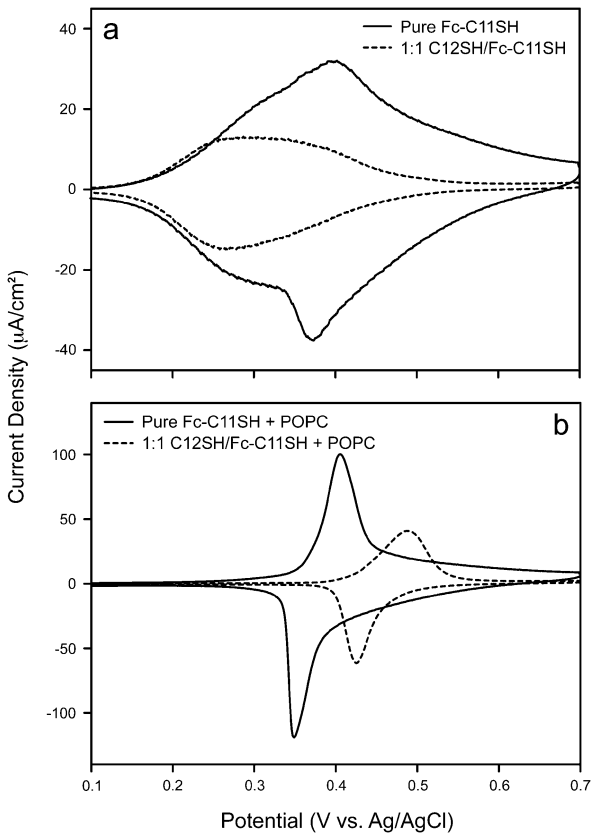

Fig. 4 Cyclic voltammograms of ferrocenyl-terminated SAMs with/without coverage of a POPC top layer. Reduction/oxidation waves of ferrocene are obtained either from SAMs alone (a) or SAMs covered with the lipid top layer (b). The SAMs are formed from either pure Fc-C11SH thiols or a 1 : 1 (mol) mixture of C12SH and Fc-C11SH thiols. A three-electrode setup with a Ag/AgCl reference electrode and a Pt counter electrode was used. Scan rate: 100 mV s^{-1}. Supporting electrolyte: 0.1 M $NaClO_4$.

The difference in shape and onset potentials of these CVs confirms that a lipid film can be successfully deposited on ferrocene-terminated SAMs. For the Fc-C11SH SAM directly exposed to the supporting electrolyte in water, the main redox wave at 0.39 V is broad and before it, there exists a small but still a noticeable shoulder wave. Such kind of peak broadening is generally attributed to the heterogeneous orientation and organization of ferrocenyl moieties in the monolayer[43,44] and accompanying these changes, a modified interfacial potential distribution.[45] One explanation of the existence of two apparent redox waves in ferrocene SAMs is based on the argument of electrostatics. When the SAM is directly immersed in aqueous media, these ferrocenyl moieties would either form clusters with their immediate neighbors in the SAM, or remain isolated. Compared to the isolated ferrocenyl groups, the oxidation of clustered ferrocenes demands higher electrochemical potential, because, electrostatically, the presence of positively charged ferrocenium ions nearby disfavors further removal of electrons from the remaining ferrocenes within the cluster.[46] In turn, the presence of two populations of ferrocenes in the SAM produces two apparent redox waves in the voltammogram. Such an electrostatic constraint is comparatively less significant in the 1 : 1 C12SH/Fc-C11SH mixed SAM, as the dilution lowers the chance of interaction among Fc-C11SH thiol molecules and thus the fraction of clustered ferrocenes. As a result, its main redox wave appears less positive to that of the pure Fc-C11SH SAM.

When these ferrocene-containing SAMs are further covered with a layer of lipids, the local dielectric environment surrounding these ferrocenyl groups is switched from water (high ε) to hydrocarbon chains of lipids (low ε), which modifies the interfacial potential distribution among different layers and thus the apparent redox potentials.[45] The fact that the potential shift and peak sharpening are also observed in THF points to the importance of local media immediately surrounding the

electroactive layer in shaping the voltammetric response of the ferrocene moieties. Once in place, moreover, the top lipid layer would also impose a mass-transfer barrier for supporting electrolyte ions to reach the ferrocenyl sites for charge compensation. The transport of ions through the lipid layer appears to be strongly lipid dependent, producing almost no potential shift when egg PC was used;[42] whereas for another bilayer formed with DMPC of two saturated C14 chains, a shift of >300 mV was observed.[47] Our result shows that the POPC top layer behaves closer to egg PC than DMPC in ferrocene-containing hybrid bilayers, which is likely related to the fluidity of these lipids at room temperature. In addition, it is evident from our result that the loading of ferrocenes in the mixed SAMs can also influence the level of potential shift.

3.5 Impedance spectroscopy

Impedance analysis was performed on C12SH and Fc-C11SH SAMs as well as SAM/POPC bilayers similar to previous studies.[23,31] As shown in Fig. 5, an increase in the circuit impedance is generally observed when the SAMs are further covered by a POPC layer. Fitting these data to a series RC circuit model, the capacitance associated with each SAM/bilayer can then be extracted (Table 1). The capacitance of the C12SH self-assembled monolayer was found to be 1.51 μF cm^{-2}, in good agreement with 1.50 μF cm^{-2} reported by Silin *et al.*[27] Furthermore, the thickness of the monolayer can be calculated from the following relationship:[23] $1/C = d/\varepsilon\varepsilon_0$, where d is the thickness of the dielectric medium that separates the two

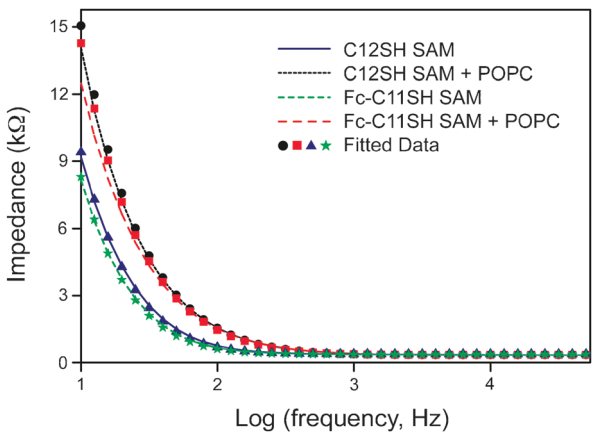

Fig. 5 Impedance spectra of C12SH and Fc-C11SH SAMs and the corresponding hybrid bilayers. Here, impedance of the films was monitored as a function of the applied ac frequency. A series-RC circuit model is used to fit the resultant cell impedance in all measurements. The fitted data are presented by four different symbols colored according to their corresponding impedance spectrum. Also see the main text.

Table 1 Effect of the C12SH SAM and the Fc-C11SH SAM on the capacitance of the POPC/thiol bilayers

	Capacitance of the SAM layer (C_{SAM})^a/μF cm^{-2}	Capacitance of the bilayer (C_{BL})^a/μF cm^{-2}	Capacitance of the lipid layer (C_{lipid})^b/μF cm^{-2}
C12SH SAM	1.51 ± 0.01	0.98 ± 0.02	2.78
Fc-C11SH SAM	1.66 ± 0.01	1.05 ± 0.02	2.86

^{a} Measured values of same samples (n = 3). ^{b} Calculated values.

Table 2 Calculated dielectric thickness of SAMs and lipid layers^a

	Dielectric thickness of the SAM layer/Å	Dielectric thickness of the POPC lipid layer/Å
C12SH SAM	13.5	8.6
Fc-C11SH SAM	12.3	8.4

^{a} ε values[23,27] of 2.3 and 2.7 were used for the alkanethiol and POPC monolayer, respectively, in the calculation.

conducting plates (*i.e.*, the gold electrode and the electrolyte solution), ε is the dielectric constant of the separating medium (*i.e.*, 2.3 for SAMs), and ε_0 is the permittivity of free space ($\varepsilon_0 \approx 8.854 \times 10^{-12}$ F m^{-1}) (Table 2). The capacitive thickness of the C12SH SAM layer was thus calculated to be 13.5 Å. By contrast, the capacitance of the Fc-C11SH SAM was measured to be 1.66 μF cm^{-2}, which corresponds to a dielectric thickness of 12.3 Å and hence is close to the C12SH SAM.

For the hybrid bilayers, the capacitance of the lipid layer alone (C_{lipid}) can be calculated from the capacitance of the bilayer (C_{BL}) and the alkanethiol SAM (C_{SAM}) layer by the following relation:[23] $C_{lipid}^{-1} = C_{BL}^{-1} - C_{SAM}^{-1}$. The capacitance of the POPC lipid monolayer formed on the C12SH SAM is determined to be 2.78 μF cm^{-2}, whereas on the Fc-C11SH SAM it is 2.86 μF cm^{-2}. In turn, these capacitance values allow the dielectric thickness of the POPC layer to be calculated: 8.6 Å (on the C12SH SAM) *vs.* 8.4 Å (on the Fc-C11SH SAM), using ε = 2.7 for POPC. These results again suggest that a monolayer quantity of POPC is formed on the ferrocene-terminated SAM as compared to its methyl-terminated counterpart.

3.6 Photocurrent generation/modulation on hybrid bilayers

Two photoactive species, monomalonic fullerene (C_{63}) and $Ru(bpy)_3^{2+}$, are separately studied in the photocurrent generation. While fullerenes are directly embedded in the POPC top layer of the hybrid bilayer by fusing C_{63}-incorporated liposomes onto preformed SAMs, $Ru(bpy)_3^{2+}$ species are introduced into the bilayer using DOPE as an anchor (Scheme 1). Consequently, when the Fc-C11SH SAM is employed as the underlying layer, the hybrid bilayers contain the photoactive component (either C_{63} or $Ru(bpy)_3^{2+}$) at the top and the redox active ferrocenes roughly at the center of the hybrid bilayer.

Fig. 6 records the photoelectrochemical action spectra of hybrid bilayers containing either $Ru(bpy)_3^{2+}$ or fullerene C_{63}. For the $Ru(bpy)_3^{2+}$-containing bilayer the maximal current was observed at ~450 nm, which matches the metal-to-ligand charge transfer electronic transitions of $Ru(bpy)_3^{2+}$–DOPE in the liposome sample; and for the C_{63}-containing bilayer, the broad photocurrent profile again follows the absorption of the fullerene-based liposome sample. The general agreement between the action spectra and the corresponding UV-vis absorption spectra thus establishes that these lipid-assembled photoactive species are responsible for the generated photocurrents.

Fig. 7 compares anodic/cathodic photocurrents generated from 2% $Ru(bpy)_3^{2+}$ deposited on either C12SH or Fc-C11SH SAMs. Under anodic conditions, an ~30% less current was consistently generated from the bilayer containing the Fc-C11SH SAM compared to that with the C12SH SAM. This difference in the obtained photocurrents should not be caused by a higher loading of $Ru(bpy)_3^{2+}$–DOPE on the C12SH SAM: when the

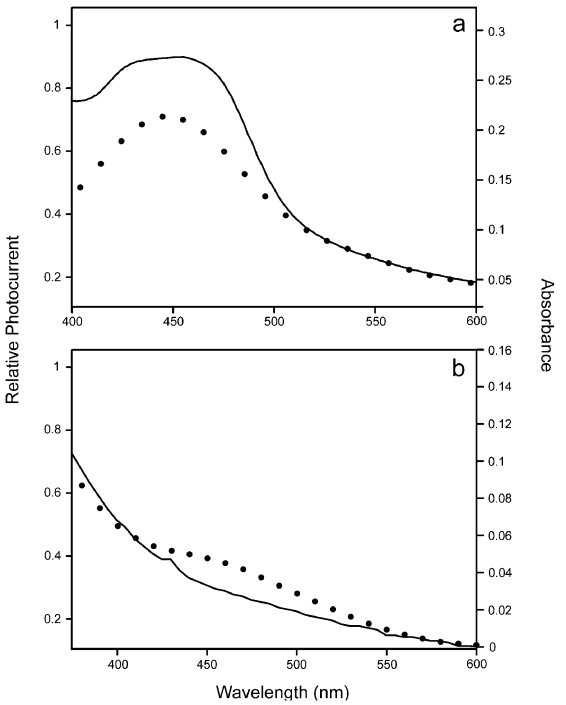

Fig. 6 Photoelectrochemical action spectra (dotted responses) of hybrid bilayers comprised of either 2% $Ru(bpy)_3^{2+}$ (a) or 2% fullerene C_{63} (b) in the POPC top layer with a Fc-C11SH SAM underlayer. The photocurrents were generated in a three-electrode cell containing 50 mM methyl viologen in HEPES buffer saline. The corresponding absorption spectra (solid lines) were obtained from 0.25 mM POPC liposome samples containing either 2% $Ru(bpy)_3^{2+}$–DOPE (a) or 2% C_{63} (b).

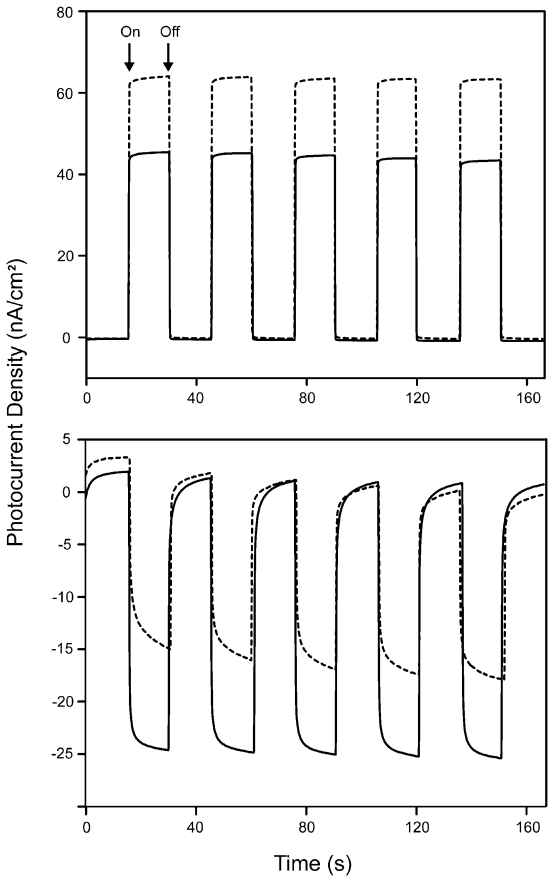

Fig. 7 Photocurrents generated from 2% $Ru(bpy)_3^{2+}$–DOPE in the POPC lipid monolayer formed on either the C12SH SAM (dashed traces) or the Fc-C11SH SAM (solid traces). The anodic photocurrents (traces in the top panel) were generated in 50 mM ascorbate dissolved in HEPES buffer (10 mM HEPES, 100 mM NaCl, pH 7.7), in which oxygen was depleted by adding 50 mM glucose, 50 units mL^{-1} glucose oxidase, and 200 units mL^{-1} catalase. (bottom) Cathodic photocurrents were obtained from 50 mM methyl viologen dissolved in the same buffer. All photocurrents were collected with the three-electrode electrochemical cell as described above; the excitation light was provided by a Hg lamp filtered at 470 ± 20 nm with an average intensity of 20 mW cm^{-2}.

same films were subjected to the cathodic photocurrent generation, an approximately 40% higher current was obtained from the Fc-C11SH SAM based bilayer (bottom panel, Fig. 7). Thus, the insertion of an electroactive ferrocene layer in between the layer of photoagents and the electrode can modulate the photocurrent generation in the bilayer-based system.

A similar trend was also observed on bilayers comprising fullerene C_{63} as the photoactive agent (Fig. 8). Here, an ~80% decrease of anodic photocurrent was seen for fullerenes immobilized on the Fc-C11SH SAM as compared to that formed on the C12SH SAM; whereas an ~4-fold enhancement in cathodic current was observed for the ferrocene-containing bilayer. Thus, a significantly stronger modulation can be achieved on fullerene-based devices compared to those based on $Ru(bpy)_3^{2+}$.

The generation and modulation of photocurrents in the present system can be understood by evaluating the energy levels and relative position of the involved species in the bilayer (Fig. 9). In the anodic process and for fullerene C_{63} immobilized on the C12SH SAM, the highly oxidizing excited-state fullerene takes one electron from ascorbate in the solution and the thus formed anion radical ($F^{\bullet -}$) then passes an electron to the gold electrode. By contrast, when the underlying layer is a Fc-C11SH SAM instead, the presence of ferrocenes in the bilayer inserts a set of new energy states along the ET pathway that photogenerated electrons may temporarily occupy. Importantly, when the gold electrode is poised at 0 V *vs.* Ag/AgCl, further transfer of electrons from these intermediate states (centered at 0.38 V) becomes a thermodynamically uphill process and thus is expected to be hindered, leading to a decrease in the anodic photocurrents. A very different scenario exists in the cathodic photocurrent generation (bottom panel, Fig. 9). Here, electrons flow out from gold first to ferrocenes and then to fullerenes. Together, these three energy levels form an overall downhill redox gradient that can facilitate cross-membrane ET processes. As theoretically analyzed by Warshel and Schlosser,[49] one way to achieve efficient light-induced ET across low dielectric matrices such as a lipid bilayer is to form a cross-membrane electrochemical gradient; in this case, the forward ET steps can effectively compete with the backward processes because of the significantly lower activation barriers associated with the forward processes. Needless to say, this general strategy is exhaustively utilized by Nature in natural photosynthesis.

A similar analysis can be raised for the $Ru(bpy)_3^{2+}$-based system. Here, the photoexcited $Ru(bpy)_3^{2+}$ first reacts with

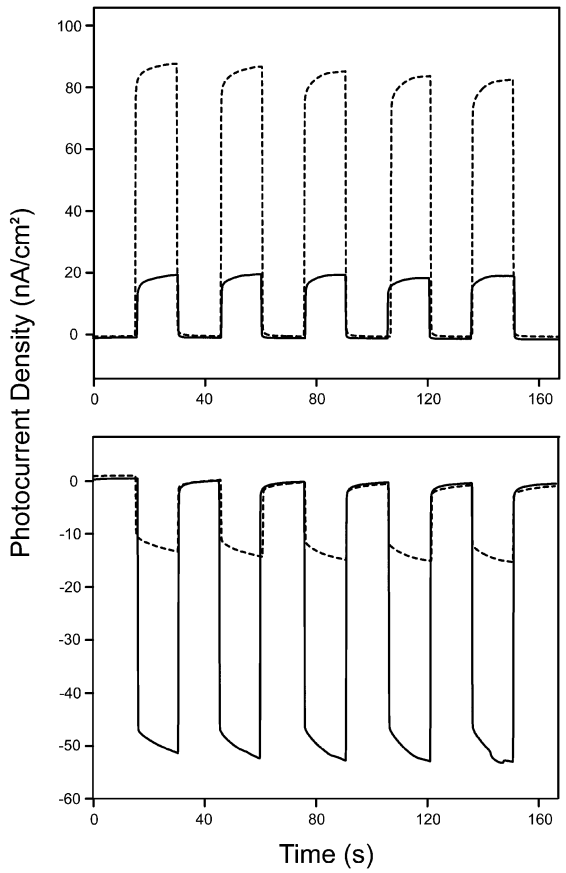

Fig. 8 Photocurrents generated from 2% fullerene C_{63} embedded in the POPC monolayer formed on either the C12SH SAM (dashed traces) or the Fc-C11SH SAM (solid traces). Conditions for anodic/cathodic photocurrent generation are identical to those of Fig. 7; the excitation light was provided by a Hg lamp filtered at 417 ± 30 nm with an average intensity of 40 mW cm^{-2}.

either ascorbate (in the anodic process) or oxygen/methyl viologen (cathodic) in the solution to give either $Ru(bpy)_3^{+}$ or $Ru(bpy)_3^{3+}$. Further electron exchange between these photogenerated species and the gold electrode is again modulated by the ferrocenes situated in between, resulting in either a decreased anodic current or an enhanced cathodic current (Fig. 9). Mechanistically, there exists a possibility that the ferrocenes in the bilayer may compete with the redox species in the solution for reacting with $Ru(bpy)_3^{2+*}$ *via* electron transfer. These processes, even if present, are expected to be relatively small, considering that the lipid-conjugated $Ru(bpy)_3^{2+}$ molecules are directly exposed to the solution redox molecules, while on the other side separated from the underlying ferrocenes by the low dielectric hydrocarbon chains of POPC. This analysis is further supported by the fluorescence spectroscopy results of $Ru(bpy)_3^{2+}$-containing bilayers. When the rate of electron transfer between $Ru(bpy)_3^{2+*}$ and an electron donor/acceptor is fast compared to that of $Ru(bpy)_3^{2+}$ fluorescence emission, quenching of $Ru(bpy)_3^{2+}$ fluorescence will result. As shown in Fig. 10, $Ru(bpy)_3^{2+}$ immobilized on the Fc-C11SH SAM displayed ~25% higher fluorescence intensity as compared to that formed on the C12SH SAM (spectra 1 and 2). Here, besides ferrocene and

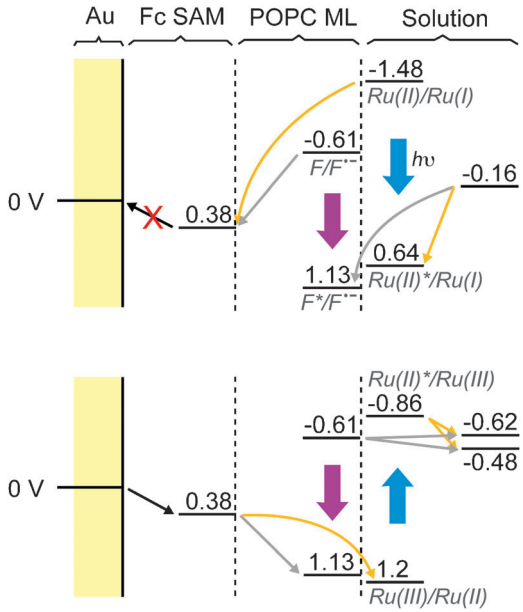

Fig. 9 Energy diagrams of electro- and photo-active species involved in the anodic (top panel) and cathodic (bottom) photocurrent generation processes. Different mediators were employed in the anodic (ascorbate at −0.16 V *vs.* Ag/AgCl) and cathodic (O_2 at −0.48 V and methyl viologen at −0.62 V) processes. The redox potential of ferrocene is obtained from Fig. 4 of this work, whereas the potentials associated with $Ru(bpy)_3^{2+}$ and fullerene are taken from ref. 31 and 48, respectively. The electron-flow pathways for $Ru(bpy)_3^{2+}$ and fullerene are indicated by arrows. Thick arrows indicate photoexcitation of the photoagents: 417 ± 30 nm for fullerene and 470 ± 20 nm for $Ru(bpy)_3^{2+}$.

ascorbate (as plausible quenchers), it is important to realize that the gold film underneath can also quench fluorescence *via* energy transfer.[50–52] For fluorophores located close to a planar metal surface, the fluorescence lifetime decays inversely to the fourth power of the fluorophore-to-metal distance.[50,51] Thus, the less fluorescence observed from $Ru(bpy)_3^{2+}$ deposited on the Fc-C11SH SAM may be attributed to the slightly larger displacement of fluorophores from the gold surface in the ferrocene-containing bilayer. From these data, it is hard to directly gauge the contribution of ferrocenes in the resulted fluorescence quenching. Nevertheless, if this contribution is dominant, it should leave little room for other quenchers to significantly quench the fluorescence. Yet, with the addition of ascorbate into the solution, the fluorescence emission was seen to decrease by ~55% on the Fc-C11SH SAM and ~65% on the C12SH SAM (spectra 3 and 4, Fig. 10), as a result of reductive quenching. These results thus indicate that the electron exchange between photoexcited $Ru(bpy)_3^{2+}$ and electron donor species in solution is more likely the initial step of the ET cascade that eventually leads to the anodic photocurrent generation (Fig. 9). A similar trend was also observed in the cathodic photocurrent generation where methyl viologen and oxygen were used as electron acceptors (ESI†, Fig. S2).

On the other hand, the consistently lower degree of photocurrent modulation seen in the $Ru(bpy)_3^{2+}$-based systems reflects the importance of size and relative position of photoagents in the bilayer in determining such a modulation effect.

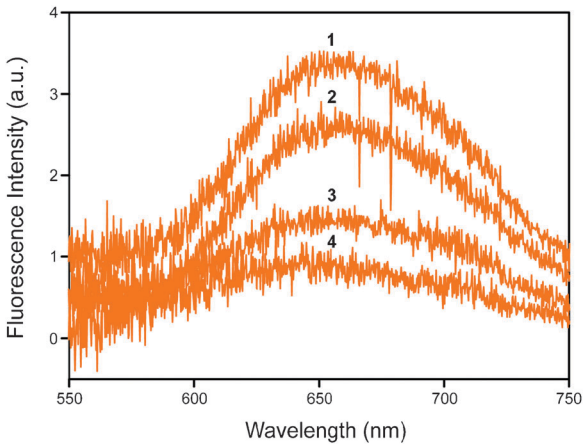

Fig. 10 Fluorescence emission spectra of 2% $Ru(bpy)_3^{2+}$–DOPE assembled in either the POPC/Fc-C11SH SAM (spectra 1 and 3) or the POPC/C12SH SAM (spectra 2 and 4) bilayers. In all samples, the oxygen was removed from the solution using an enzymatic cocktail solution containing glucose oxidase, catalase and glucose (see the Experimental section). Of these, samples used to acquire spectra 2 and 4 in addition contained 50 mM ascorbate. Excitation was made at 470 ± 20 nm.

As we discussed previously,[30,32] the hydrophobic bulk of the amphiphilic fullerene C_{63} is believed to be buried in the hydrocarbon region of the lipid layer, whereas the DOPE-conjugated $Ru(bpy)_3^{2+}$ moieties are relatively hydrophilic and thus should stick up from the lipid/water interface and directly face the initial layers of the aqueous phase. Consequently, the differences in location and size of the two agents render the fullerenes to be positioned closer to the underlying ferrocenes, which gives rise to a stronger electronic coupling between the two and thus a larger change in photocurrents as compared to the case of $Ru(bpy)_3^{2+}$.

Previous studies have detailed several other approaches of using ferrocene derivatives to modulate photocurrents in layered architectures. For example, by using the Langmuir–Blodgett deposition technique to organize amphiphilic polymers containing either $Ru(bpy)_3^{2+}$ or ferrocene moieties on electrodes, Miyashita and coworkers[53] found that the direction of photocurrents depends on the deposition order of the redox polymers on electrodes. By further connecting the anodic and cathodic films in series and altering the deposition order of the two components, logic operations such as 'OR' and 'XOR' could also be realized.[54] In another self-assembly based study, Matsuo and colleagues[55] synthesized penta(carboxylic) ferrocene–fullerene complexes that could be directionally immobilized on indium tin oxide electrodes. The close distance between the ferrocene and fullerene in the complex afforded a complete rectification of the obtained photocurrents. In comparison, a complete rectification of anodic photocurrent is not seen in the present system, even for just 2% fullerene C_{63} immobilized on the pure Fc-C11SH SAM, which may be caused by the following factors. First of all, compared to the system studied by Matsuo *et al.*,[55] the distance between fullerene and ferrocene in our system is still not ideal for maximal electronic coupling. Further, the non-idealness in packing and assembly of the SAMs and lipids, *e.g.*, as shown in Fig. 3, may introduce additional pathways to the photoinduced ET processes across these bilayers. Finally, it is also conceivable that gold electrodes used in this study may play a role in the occurrence of leakage photocurrents, considering the differences in their interfacial electronic characteristics and band structure as compared to the semiconducting indium tin oxide employed in their work.

4. Conclusions

We have demonstrated here that lipid monolayers can be formed on pure ferrocene-terminated C11-alkanethiol SAMs similar to their alkanethiol counterparts. When photoagents are incorporated into such bilayers, modulation of photocurrents is resulted. Such a modulation effect was found to be dependent on the distance between the photoagents and ferrocene moieties in the bilayer. Considering the scope and flexibility of lipid-based amphiphilic assembly, this lipid/SAM hybrid system should be found useful in the study of several aspects of photoinduced cross-membrane ET processes, including various physiochemical parameters (*e.g.*, distance and energetics) and other interfacial properties that can influence the ET efficiency.

Acknowledgements

This work is supported by the NSF (CHE-0951743), USDA (through AUDFS) and Auburn University.

Notes and references

1 J. H. Fendler, Photochemical Solar Energy Conversion. An Assessment of Scientific Accomplishments, *J. Phys. Chem.*, 1985, **89**, 2730–2740.
2 H. Imahori, Y. Mori and Y. Matano, Nanostructured Artificial Photosynthesis, *J. Photochem. Photobiol., C*, 2003, **4**, 51–83.
3 S. Fukuzumi, Development of Bioinspired Artificial Photosynthetic Systems, *Phys. Chem. Chem. Phys.*, 2008, **10**, 2283–2297.
4 J. H. Fendler, *Membrane Mimetic Chemistry*, John Wiley & Sons, Inc., New York, ch. 5, 1982.
5 S. V. Lymar, V. N. Parmon and K. I. Zamaraev, Photoinduced Electron Transfer across Membranes, *Top. Curr. Chem.*, 1991, **159**, 1–65.
6 M. Calvin, Simulating Photosynthetic Quantum Conversion, *Acc. Chem. Res.*, 1978, **10**, 369–374.
7 W. E. Ford, J. W. Otvos and M. Calvin, Photosensitized Electron Transport across Lipid Vesicle Walls—Quantum Yield Dependence on Sensitizer Concentration, *Proc. Natl. Acad. Sci. U. S. A.*, 1979, **76**, 3590–3593.
8 C. Laane, W. E. Ford, J. W. Otvos and M. Calvin, Photosensitized Electron-Transport across Lipid Vesicles Walls—Enhancement of Quantum Yield by Ionophores and Transmembrane Potentials, *Proc. Natl. Acad. Sci. U. S. A.*, 1981, **78**, 2017–2020.
9 J. H. Fendler, Surfactant Vesicles as Membrane Mimetic Agents: Characterization and Utilization, *Acc. Chem. Res.*, 1980, **13**, 7–13.
10 M. S. Tunuli and J. H. Fendler, Aspects of Artificial Photosynthesis. Photosensitized Electron Transfer across Bilayers, Charge Separation, and Hydrogen Production in Anionic Surfactant Vesicles, *J. Am. Chem. Soc.*, 1981, **103**, 2507–2513.
11 S. Baral and J. H. Fendler, Cadmium Sulfide Mediated Photoelectric Effects in Bilayer Lipid Membranes, *J. Am. Chem. Soc.*, 1989, **111**, 1604–1614.
12 D. Gust, T. A. Moore and A. L. Moore, Molecular Mimicry of Photosynthetic Energy and Electron Transfer, *Acc. Chem. Res.*, 1993, **26**, 198–205.
13 D. Gust, T. A. Moore and A. L. Moore, Mimicking Photosynthetic Solar Energy Transduction, *Acc. Chem. Res.*, 2001, **34**, 40–48.
14 G. Steinberg-Yfrach, P. A. Liddell, S.-C. Hung, A. L. Moore, D. Gust and T. A. Moore, Conversion of Light Energy to Proton

Potential in Liposomes by Artificial Photosynthetic Reaction Centers, *Nature*, 1997, **385**, 239–241.
15 G. Steinberg-Yfrach, J.-L. Rigaud, E. N. Durantini, A. L. Moore, D. Gust and T. A. Moore, Light-Driven Production of ATP Catalyzed by F0F1-ATP Synthase in an Artificial Photosynthetic Membrane, *Nature*, 1998, **392**, 479–482.
16 J. N. Robinson and D. J. Cole-Hamilton, Electron Transfer across Vesicle Bilayers, *Chem. Soc. Rev.*, 1991, **20**, 49–94.
17 A. A. Brian and H. M. McConnell, Allogeneic Stimulation of Cytotoxic T Cells by Supported Planar Membranes, *Proc. Natl. Acad. Sci. U. S. A.*, 1984, **81**, 6159–6163.
18 L. K. Tamm and H. M. McConnell, Supported Phospholipid Bilayers, *Biophys. J.*, 1985, **47**, 105–113.
19 S. G. Boxer, Molecular Transport and Organization in Supported Lipid Membranes, *Curr. Opin. Chem. Biol.*, 2000, **4**, 704–709.
20 J. T. Groves and S. G. Boxer, Micropattern Formation in Supported Lipid Membranes, *Acc. Chem. Res.*, 2002, **35**, 149–157.
21 E. Sackmann, Supported Membranes: Scientific and Practical Applications, *Science*, 1996, **271**, 43–48.
22 M. Tanaka and E. Sackmann, Polymer-Supported Membranes as Models of the Cell Surface, *Nature*, 2005, **437**, 656–663.
23 A. L. Plant, Self-Assembled Phospholipid/Alkanethiol Biomimetic Bilayers on Gold, *Langmuir*, 1993, **9**, 2764–2767.
24 C. W. Meuse, G. Niaura, M. L. Lewis and A. L. Plant, Assessing the Molecular Structure of Alkanethiol Monolayers in Hybrid BilayerMembranes with Vibrational Spectroscopies, *Langmuir*, 1998, **14**, 1604–1611.
25 S. Krueger, C. W. Meuse, C. F. Majkrzak, J. A. Dura, N. F. Berk, M. Tarek and A. L. Plant, Investigation of Hybrid Bilayer Membranes with Neutron Reflectometry: Probing the Interactions of Melittin, *Langmuir*, 2001, **17**, 511–521.
26 E.-K. Sinner and W. Knoll, Functional Tethered Membranes, *Curr. Opin. Chem. Biol.*, 2001, **5**, 705–711.
27 V. I. Silin, H. Wieder, J. T. Woodward, G. Valincius, A. Offenhausser and A. L. Plant, The Role of Surface Free Energy on the Formation of Hybrid Bilayer Membranes, *J. Am. Chem. Soc.*, 2002, **124**, 14676–14683.
28 A. N. Parikh, J. D. Beers, A. P. Shreve and B. I. Swanson, Infrared Spectroscopic Characterization of Lipid–Alkylsiloxane Hybrid Bilayer Membranes at Oxide Substrates, *Langmuir*, 1999, **15**, 5369–5381.
29 M. C. Howland, A. R. Sapuri-Butti, S. S. Dixit, A. M. Dattelbaum, A. P. Shreve and A. N. Parikh, Phospholipid Morphologies on Photochemically Patterned Silane Monolayers, *J. Am. Chem. Soc.*, 2005, **127**, 6752–6765.
30 W. Zhan and K. Jiang, A Modular Photocurrent Generation System Based on Phospholipid-Assembled Fullerenes, *Langmuir*, 2008, **24**, 13258–13261.
31 K. Jiang, H. Xie and W. Zhan, Photocurrent Generation from $Ru(bpy)_3^{2+}$ Immobilized on Phospholipid/Alkanethiol Hybrid Bilayers, *Langmuir*, 2009, **25**, 11129–11136.
32 W. Zhan, K. Jiang, M. D. Smith, H. E. Bostic, M. D. Best, M. L. Auad, J. V. Ruppel, C. Kim and X. P. Zhang, Photocurrent Generation from Porphyrin/Fullerene Complexes Assembled in a Tethered Lipid Bilayer, *Langmuir*, 2010, **26**, 15671–15679.
33 D. A. Buttry and M. D. Ward, Measurement of Interfacial Processes at Electrode Surfaces with the Electrochemical Quartz Crystal Microbalance, *Chem. Rev.*, 1992, **92**, 1355–1379.
34 In this equation, Δf is the observed frequency shift (Hz), Δm is the change in mass per unit area (g cm^{-2}) and C_f is the sensitivity factor for the crystal (*i.e.*, 56.6 Hz μg^{-1} cm^2 for a 5-MHz AT-cut quartz crystal at room temperature).
35 L. V. Rajakovic, B. A. Cavic-Vlasak, V. Ghaemmaghami, K. M. R. Kallury, A. L. Kipling and M. Thompson, *Anal. Chem.*, 1991, **63**, 615–621.
36 R. Borjas and D. A. Buttry, Solvent Swelling Influences the Electrochemical Behavior and Stability of Thin Films of Nitrated Poly(styrene), *J. Electroanal. Chem.*, 1990, **280**, 73–90.
37 T. H. Ha and K. Kim, Adsorption of Lipid Vesicles on Hydrophobic Surface Investigated by Quartz Crystal Microbalance, *Langmuir*, 2001, **17**, 1999–2007.
38 H. H. Strain, M. R. Thomas and J. J. Katz, Spectral Absorption Properties of Ordinary and Fully Deuterated Chlorophylls a and b, *Biochim. Biophys. Acta*, 1963, **75**, 306–311.
39 J. K. Hurley and G. Tollin, Photochemical Energy Conversion in Chlorophyll-Containing Lipid Bilayer Vesicles, *Sol. Energy*, 1982, **28**, 187–196.
40 J. B. Hubbard, V. Silin and A. L. Plant, Self-Assembly Driven by Hydrophobic Interactions at Alkanethiol Monolayers: Mechanism of Formation of Hybrid Bilayer Membranes, *Biophys. Chem.*, 1998, **75**, 163–176.
41 A. L. Plant, Supported Hybrid Bilayer Membranes as Rugged Cell Membrane Mimics, *Langmuir*, 1999, **15**, 5128–5135.
42 A. T. A. Jenkins and J.-F. Le-Meur, Lipid Vesicle Adsorption on Electroactive Self-Assembled Monolayers, *Electrochem. Commun.*, 2004, **6**, 373–377.
43 C. E. D. Chidsey, C. R. Berotozzi, T. M. Putvinski and A. M. Mujsce, Coadsorption of Ferrocene-Terminated and Unsubstituted Alkanethiols on Gold: Electroactive Self-Assembled Monolayers, *J. Am. Chem. Soc.*, 1990, **112**, 4301–4306.
44 G. K. Rowe and S. E. Creager, Redox and Ion-Pairing Thermodynamics in Self-Assembled Monolayers, *Langmuir*, 1991, **7**, 2307–2312.
45 C. P. Smith and H. S. White, Theory of the Interfacial Potential Distribution and Reversible Voltammetric Response of Electrodes Coated with Electroactive Molecular Films, *Anal. Chem.*, 1992, **64**, 2398–2405.
46 L. Y. S. Lee, T. C. Sutherland, S. Rucareanu and R. B. Lennox, Ferrocenylalkylthiolates as a Probe of Heterogeneity in Binary Self-Assembled Monolayers on Gold, *Langmuir*, 2006, **22**, 4438–4444.
47 M. Twardowski and R. G. Nuzzo, Molecular Recognition at Model Organic Interfaces: Electrochemical Discrimination Using Self-Assembled Monolayers (SAMs) Modified via the Fusion of Phospholipid Vesicles, *Langmuir*, 2003, **19**, 9781–9791.
48 H. Imahori, T. Azuma, A. Ajavakom, H. Norieda, H. Yamada and Y. Sakata, An Investigation of Photocurrent Generation by Gold Electrodes Modified with Self-Assembled Monolayers of C_{60}, *J. Phys. Chem. B*, 1999, **103**, 7233–7237.
49 A. Warshel and D. W. Schlosser, Electrostatic Control of the Efficiency of Light-Induced Electron Transfer across Membranes, *Proc. Natl. Acad. Sci. U. S. A.*, 1981, **78**, 5564–5568.
50 H. Kuhn, Classical Aspects of Energy Transfer in Molecular Systems, *J. Chem. Phys.*, 1970, **53**, 101–108.
51 A. P. Alivisatos, D. H. Waldeck and C. B. Harris, Nonclassical Behavior of Energy Transfer from Molecules to Metal Surfaces: Biacetyl($^3n\pi^*$)/Ag(111), *J. Chem. Phys.*, 1985, **82**, 541–547.
52 M. Jebb, P. K. Sudeep, P. Pramod, K. G. Thomas and P. V. Kamat, Ruthenium(II) Trisbipyridine Functionalized Gold Nanorods. Morphological Changes and Excited-State Interactions, *J. Phys. Chem. B*, 2007, **111**, 6839–6844.
53 A. Aoki, Y. Abe and T. Miyashita, Effective Photoinduced Electron Transfer in Hetero-Deposited Redox Polymer LB Films, *Langmuir*, 1999, **15**, 1463–1469.
54 J. Matsui, K. Abe, M. Mitsuishi, A. Aoki and T. Miyashita, Quasi-Solid-State Optical Logic Devices Based on Redox Polymer Nanosheet Assembly, *Langmuir*, 2009, **25**, 11061–11066.
55 Y. Matsuo, K. Kanaizuka, K. Matsuo, Y.-W. Zhong, T. Nakae and E. Nakamura, Photocurrent-Generating Properties of Organometallic Fullerene Molecules on an Electrode, *J. Am. Chem. Soc.*, 2008, **130**, 5016–5017.